Quantum Monte Carlo with the Langevin Equation: Coupled Bose-Fermi Systems

IOP Conf. Series: Journal of Physics: Conf. Series **1290** (2019) 012004 doi:10.1088/1742-6596/1290/1/012004

Quantum Monte Carlo with the Langevin Equation: Coupled Bose-Fermi Systems

G. George Batrouni

Université Côte d'Azur, INPHYNI, CNRS, 0600 Nice, France
MajuLab, CNRS-UCA-SU-NUS-NTU International Joint Research Unit, 117542 Singapore
Centre for Quantum Technologies, National University of Singapore, 117542 Singapore
Beijing Computational Science Research Center, Beijing 100193, China

Richard T. Scalettar

Department of Physics, University of California, Davis, California 95616, USA

Abstract. We describe the algorithmic details and a performance evaluation of a Langevin approach to a strongly interacting electron-phonon system, and show it has a near linear scaling with lattice size N_s. Many of the limitations of previous attempts to employ such methods to condensed matter lattice Hamiltonians are absent. In particular, the iterative linear algebra solution remains well behaved at strong coupling and low temperatures. The use of Fourier Acceleration is crucial for efficiency, and its use makes the method competitive with the widely-used local update methods, which scale as N_s^3 for on-site interactions and N_s^4 for long range electron-phonon coupling, even on rather small lattice sizes.

1. Introduction

Monte Carlo methods for interacting classical and quantum systems are generally most easily formulated with local moves which update a single degree of freedom at a time. This has the advantage of simplicity of coding, ease of ensuring detailed balance is satisfied, and low computational cost in evaluating the change in energy required for the acceptance/rejection step. There is, however, a major drawback. Changing the field at a single coordinate, or a collection thereof, yields a new configuration which is highly correlated with its predecessors. Many such moves are required before an independent configuration is attained. This problem becomes increasingly challenging with larger lattice sizes and in the vicinity of second order phase transitions, where the correlation length diverges.

Algorithms which change many degrees of freedom at a time will be effective in solving this problem only if the cost to evaluate the energy change is not exorbitant, and also if the acceptance rate for the large proposed change is reasonably high. In certain situations, highly efficient 'cluster moves' have been formulated. The most famous examples are the Wolff and Swendsen-Wang approaches to the Ising model, which combine all the desiderata of simplicity, high acceptance rates, and inexpensive accept-reject decision [1, 2, 3]. "Loop" and "worm" methods have extended large scale moves to Quantum Monte Carlo (QMC) for bosons and quantum spins within the context of world line, stochastic series expansion, and related approaches [4, 5, 6, 7].

Simulations of quantum *fermionic* systems which move many degrees of freedom simultaneously have achieved great success in the lattice gauge theory community, and are used there almost universally. Their application to condensed matter has been more problematic. One reason is the relatively high efficiency of local-move based approaches. The cost of evaluation the change in the fermionic action scales only as the square of the spatial system size N_s for local moves, as opposed to the naive $\mathcal{O}(N_s^3)$ expectation for the evaluation of the fermion determinant. Global moves which require explicit $\mathcal{O}(N_s^3)$ evaluation of the determinant must overcome the factor of N_s increase in computational cost. The second reason is that the matrices used in molecular dynamics and Langevin algorithms become ill-conditioned. As a consequence, the solution of the linear algebra kernel gets very expensive, or simply fails [8, 9, 10, 11].

The advent of "machine learning" has lent many new perspectives to the field, including more efficient updates, recognition of phases, and even the sign problem [12, 13, 14, 15]. In particular, self-learning Monte Carlo (SLMC) [16, 17, 18, 19] has been shown to generate moves which provide large changes to the configuration at low computation cost and with high acceptance rates. Originally formulated for classical models, SLMC has now been developed for fermionic systems [20]. The key concept is leveraging inexpensive simulations on small lattices which use the full determinant to generate a determinant-free effective model with an energy which can be very rapidly evaluated, but which is close enough to the original model that moves are accepted with high probability. Somewhat remarkably, simulations on these small lattices are found to produce models which remain accurate even when large lattices are studied.

2. Model and algorithm

In this paper we return to the lattice gauge theory (LGT) idea of using Langevin dynamics to generate and sample equilibrium configurations of a quantum system [21, 22, 23, 24]. We show that there is a class of Hamiltonians for which such approaches are very promising. These involve models of electrons, with creation (destruction) operators $\hat{c}^\dagger_{j\sigma}(\hat{c}_{j\sigma})$ on site j and with spin σ, coupled to phonon degrees of freedom $\hat{a}^\dagger_j(\hat{a}_j)$:

$$\begin{aligned}\hat{H} = &-t\sum_{\langle ij\rangle\sigma}\left(\hat{c}^\dagger_{i\sigma}\hat{c}_{j\sigma}+\hat{c}^\dagger_{j\sigma}\hat{c}_{i\sigma}\right)-\mu\sum_{i\sigma}\hat{n}_{i\sigma},\\ &+\omega_0\sum_i(\hat{a}^\dagger_i\hat{a}_i+\frac{1}{2})+g\sum_{i,r,\sigma}f(r)(\hat{a}^\dagger_i+\hat{a}_i)\,\hat{c}^\dagger_{i+r,\sigma}\,\hat{c}_{i+r,\sigma}\end{aligned} \tag{1}$$

Here t is the kinetic energy scale of the fermions, which we set to $t=1$ as our unit of energy, and $\langle ...\rangle$ denotes near neighbors. ω_0 is the bare boson energy scale, and $gf(r)$ is the coupling of bosons on site i with fermions on site $i+r$. We choose a specific form $f(r)=e^{-r/\xi}/(1+r^2)^{3/2}$ derived by Fröhlich [25] which is appropriate to electron-phonon interactions. The phonon operators are related to the nuclear position and momentum by

$$\hat{x}_j=\frac{1}{\sqrt{2\omega_0}}\left(\hat{a}^\dagger_j+\hat{a}_j\right),\quad \hat{p}_j=\frac{1}{i}\sqrt{\frac{\omega_0}{2}}\left(\hat{a}_j-\hat{a}^\dagger_j\right). \tag{2}$$

The partition function of the system is given by $\mathcal{Z}=\mathrm{Tr}\,e^{-\beta\hat{H}}=\mathrm{Tr}e^{-\Delta\tau\hat{H}}e^{-\Delta\tau\hat{H}}\ldots e^{-\Delta\tau\hat{H}}$, where we have discretized the imaginary time direction (*i.e.* β) such that $\beta=\Delta\tau L_\tau$ with L_τ the number of discrete steps. The partition function is expressed as a path integral over nuclear positions by inserting complete sets of coordinate and momentum states between each pair of exponentials and integrating out the momenta. Since the Hamiltonian is quadratic in

the fermion operators, the trace can be performed exactly leading to [26],

$$\mathcal{Z} = \int \mathcal{D}\, x(i,\tau)\; e^{-S_{\rm bose}}\; \left(\det M(\{x(i,\tau)\}\right)^2 \tag{3}$$
$$S_{\rm bose} = \frac{1}{2}\Delta\tau\omega_0^2 \sum_{i,\tau} x(i,\tau)^2 + \frac{1}{2}\Delta\tau \sum_{i,\tau} \left(\frac{x(i,\tau+1)-x(i,\tau)}{\Delta\tau}\right)^2.$$

The fermion matrix, $M\left(\{x(i,\tau)\}\right)$ depends on the phonon field, $\{x(i,\tau)\}$, which is space and imaginary-time dependent. We note that the square of the determinant can be written in the form $\det\left(M^T M\right)$ which will be used in what follows. As is well known [27], the determinant can be written as $\det M = \det\left[I + B_{L_\tau} \ldots B_3 B_2 B_1\right]$ where B_ℓ is the $N_s \times N_s$ matrix, $B_\ell = \mathrm{e}^{-\mathrm{d}\tau k}\mathrm{e}^{-\mathrm{d}\tau v_\ell}$. N_s is the number of sites, and, for a one-d chain with near-neighbor hopping,

$$k = -\begin{bmatrix} \mu & t & 0 & 0 & \ldots & 0 & t \\ t & \mu & t & 0 & \ldots & 0 & 0 \\ 0 & t & \mu & t & \ldots & 0 & 0 \\ \ldots & \ldots & \ldots & \ldots & \ldots & \ldots & \ldots \\ t & 0 & 0 & 0 & \ldots & t & \mu \end{bmatrix}, \tag{4}$$

and

$$v_\ell = -\begin{bmatrix} x_g(1,\ell) & 0 & 0 & 0 & \ldots & 0 \\ 0 & x_g(2,\ell) & 0 & 0 & \ldots & 0 \\ 0 & 0 & x_g(3,\ell) & 0 & \ldots & 0 \\ \ldots & \ldots & \ldots & \ldots & \ldots & \ldots \\ 0 & 0 & 0 & 0 & \ldots & x_g(N_s,\ell) \end{bmatrix}. \tag{5}$$

The term $x_g(j,\ell)$ in the interaction matrix v_ℓ is defined by

$$x_g(j,\ell) = g \sum_{k=1}^{N_s} f(j+k)x(k,\ell), \tag{6}$$

which includes the interaction of site j with all other sites according to Eq.(1).

Instead of performing a single-site Monte Carlo update of the phonon field, we first write Eq.(3) as,

$$\mathcal{Z} = \int \mathcal{D}\, x(i,\tau)\; e^{-S}, \tag{7}$$
$$S = S_{\rm bose} - \ln\left(\det(M^T M)\right), \tag{8}$$

and we define fictitious evolution dynamics governed by the Langevin equation,

$$\frac{\mathrm{d}x(j,\tau,t)}{\mathrm{d}t} = -\frac{\partial S}{\partial x(j,\tau,t)} + \sqrt{2}\,\eta(j,\tau,t), \tag{9}$$

with the stochastic variable η satisfying

$$\langle \eta(j,\tau,t)\rangle = 0 \qquad \langle \eta(j,\tau,t)\eta(r,\tau',t')\rangle = \delta_{j,r}\delta_{\tau,\tau'}\delta(t-t'). \tag{10}$$

j labels the spatial coordinate of a site, τ its imaginary time and t the Langevin time. In the stationary limit, after transients have died out, the configurations generated by this equation are indeed governed by the Boltzmann weight e^{-S} [21, 28].

We discretize the Langevin time in order to integrate Eq.(9) numerically,

$$\begin{aligned} x(j,\tau,t+\mathrm{d}t) &= x(j,\tau,t) - \mathrm{d}t\frac{\partial S}{\partial x(j,\tau,t)} \\ &\quad +\sqrt{2\mathrm{d}t}\,\eta(j,\tau,t), \end{aligned} \tag{11}$$

with $\langle\eta(j,\tau,t)\rangle = 0$ and $\langle\eta(j,\tau,t)\eta(r,\tau',t')\rangle = \delta_{j,r'}\delta_{\tau,\tau'}\delta_{t,t'}$, which can be modeled with Gaussian random numbers, the discrete analogs of Eq. 10. Here we used the simplest (Euler) discretization, and note the square root of the Langevin time step, $\mathrm{d}t$, in Eq. (11) which comes from replacing the Dirac δ-function in Eq. (10) by the discrete Kronecker form, $\delta(t-t') \to \delta_{t,t'}/\mathrm{d}t$. This results in the linear systematic error $\mathcal{O}(\mathrm{d}t)$ as opposed to $\mathcal{O}(\mathrm{d}t^2)$ for deterministic differential equations. One can, instead, use Runge-Kutta discretization [21] to reduce the errors to $\mathcal{O}(\mathrm{d}t^2)$ here too, but we have found the Euler discretization to be sufficiently accurate (see below).

The derivative of the action in Eq.(11) can be easily calculated,

$$\frac{\partial S}{\partial x(j,\tau,t)} = \frac{\partial S_{\mathrm{bose}}}{\partial x(j,\ell,t)} - 2\,\mathrm{Tr}\left(\frac{\partial M}{\partial x(j,\ell,t)}M^{-1}\right). \tag{12}$$

To avoid the costly computation of the trace term, we note that, given a vector of Gaussian random numbers, $\vec{g}$, we have $\langle\vec{g}^T A\vec{g}\rangle = \mathrm{Tr}A$, where the average is taken over the Gaussian distribution. We, therefore, replace the trace term by such a stochastic estimator and write,

$$\frac{\partial S}{\partial x(j,\tau,t)} = \frac{\partial S_{\mathrm{bose}}}{\partial x(j,\tau,t)} - 2\vec{g}^T\left(\frac{\partial M}{\partial x(j,\ell,t)}M^{-1}\right)\vec{g}. \tag{13}$$

At first sight it may appear that we have not gained much because we still need to perform the costly calculation of M^{-1}. However, this is not so since we only need $M^{-1}\vec{g}$ which is calculated by solving $M\vec{x} = \vec{g}$ using the bi-Conjugate Gradient (bCG) algorithm. The number of bCG iterations is set by the tolerance level (typically we take $10^{-4} \sim 10^{-5}$), and also by the other physical parameters of the problem (discussed below). Note that in this algorithm, the entire phonon field, $x(j,\tau)$, is updated in a single Langevin step. All the operations are simple sparse matrix-vector multiplies which can be easily optimized.

A well known problem facing simulations of electron-phonon systems is the very long auto-correlation times. To mitigate this difficulty, we introduce Fourier Acceleration (FA) of the Langevin dynamics. The idea is that different length scales can evolve at different rates. Our goal is to force them to evolve at, more or less, the same rate. To implement this, we note that for an arbitrary positive definite matrix, Q, the stationary state configurations produced by the generalized Langevin equation,

$$\frac{\mathrm{d}\vec{x}(t)}{\mathrm{d}t} = -Q\frac{\mathrm{d}S}{\mathrm{d}\vec{x}(t)} + \sqrt{2Q}\,\vec{\eta}(t), \tag{14}$$

are guaranteed to have the correct Boltzmann weigh, e^{-S}. Our aim, then, is to find a Q which is inexpensive to compute and which reduces the autocorrelation times. The form we choose is inspired by the noninteracting limit, $g = 0$ where we have:

$$\frac{\mathrm{d}S}{\mathrm{d}x(i,\tau)} = \Delta\tau\,\omega_0^2 x(i,\tau) + \frac{[x(i,\tau+1) + x(i,\tau-1) - 2x(i,\tau)]}{\Delta\tau}, \tag{15}$$

which becomes, after Fourier transforming along imaginary time,

$$\frac{\mathrm{d}\tilde{S}}{\mathrm{d}\tilde{x}(i,k_\tau)} = \left(\Delta\tau\,\omega_0^2 + [2 - 2\cos(2\pi k_\tau/L_\tau)]/\Delta\tau\right)\tilde{x}(i,k_\tau), \tag{16}$$

with $-L_\tau/2 + 1 \leq k_\tau \leq L_\tau/2$. The ratio of the slowest to fastest mode is $(\Delta\tau\,\omega_0)^2/\left(4+(\Delta\tau\,\omega_0)^2\right) \ll 1$, exposing the critical slowing down of the phonons in the imaginary time direction, which gets worse for smaller $\Delta\tau$ and ω_0. To compensate for this, we choose the matrix Q to be diagonal in imaginary time Fourier space and given by,

$$\tilde{Q}(k_\tau) = \frac{\Delta\tau\omega_0^2 + 4/\Delta\tau}{\Delta\tau\omega_0^2 + (2-2\cos(2\pi k_\tau/L_\tau))/\Delta\tau}, \tag{17}$$

which is normalized so that $\tilde{Q}(L_\tau/2) = 1$. This choice shows clearly that the fastest mode is not accelerated, it does not need to be, and the slower the mode the stronger the acceleration gets. In the noninteracting limit, this choice will totally eliminate critical slowing down. This is not true when $g \neq 0$. Nonetheless we find that this form, motivated by the noninteracting limit, is inexpensive to calculate, works very well and helps convergence even in the strongly interacting case. We, therefore, use Eq. (17) in all the follows.

The Fourier accelerated Langevin equation then becomes,

$$\begin{aligned}\frac{\mathrm{d}\vec{x}(t)}{\mathrm{d}t} &= -\hat{\mathbf{F}}^{-1}\tilde{Q}(k_\tau)\hat{\mathbf{F}}\frac{\mathrm{d}S}{\mathrm{d}\vec{x}(t)} + \hat{\mathbf{F}}^{-1}\sqrt{2\tilde{Q}(k_\tau)}\,\hat{\mathbf{F}}\vec{\eta}(t) \\ &= -\hat{\mathbf{F}}^{-1}\left[\tilde{Q}(k_\tau)\hat{\mathbf{F}}\frac{\mathrm{d}S}{\mathrm{d}\vec{x}(t)} + \sqrt{2\tilde{Q}(k_\tau)}\,\hat{\mathbf{F}}\vec{\eta}(t)\right],\end{aligned} \tag{18}$$

where $\hat{\mathbf{F}}$ is an FFT operator, $\tilde{Q}(k_\tau)$ is given by Eq. (17), and $\mathrm{d}S/\mathrm{d}\vec{x}$ is given by Eq. (13). In what follows, we use this equation with the simple Euler discretization of the Langevin time.

Physical phonon quantities can be easily calculated since the QMC evolves the phonon field directly. All fermionic quantities can be calculated once the Green function is obtained by,

$$G(i,j) = \left\langle (M[\{x\}])^{-1}_{i,j} \right\rangle, \tag{19}$$

where the sites i and j can be at equal or unequal imaginary time. Indeed, an additional advantage of the Langevin approach is that one does not need separate (and computationally costly) routines to evaluate the unequal time Green function. As we did in the update steps, we avoid evaluating M^{-1} by using a stochastic estimator, to calculate the Green function

$$G(i,j) = \left\langle \gamma_i \left(M[\{x\}]^{-1}\vec{\gamma}\right)_j \right\rangle, \tag{20}$$

where γ_j is a Gaussian random number. $M^{-1}\vec{\gamma}$ is calculated with the bCG algorithm. Once $G(i,j)$ is available, all fermionic quantities, *e.g.* kinetic energy, density correlations, structure factor etc, can be obtained.

3. Benchmarking the Algorithm

We now study the performance of the algorithm and assess how well it works compared with determinant quantum Monte Carlo (DQMC). We will examine the systematic errors due to the discretization of imaginary time and Langevin time in addition to the benefits of Fourier acceleration and the scaling of computation time as a function of the system size. We focus on the charge density wave structure factor,

$$S(\pi,\pi) = \frac{1}{N_s}\sum_{i,j}\langle n(i)n(j)\rangle\,(-1)^{i+j}\ , \tag{21}$$

which sums the density correlations over the entire spatial lattice with a phase $(-1)^{i+j}$ which is +1 if the sites are on the same sublattice, and -1 if they are on different sublattices, of the

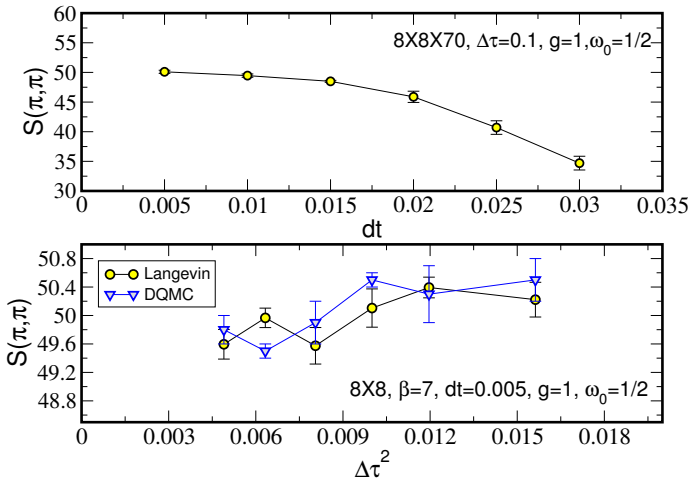

Figure 1. (Color online) Top: The dependence of the structure factor, $S(\pi, \pi)$, on the Langevin time step, $\mathrm{d}t$, in the ordered phase. For $\mathrm{d}t \leq 0.015$ the discretization error becomes linear in $\mathrm{d}t$. Bottom: The dependence of $S(\pi, \pi)$ on the imaginary time step, $\Delta\tau$, for both DQMC and Langevin. The Trotter-Suzuki errors are comparable in the two algorithms. $\mathrm{d}t = 0.005$ used to integrate the Langevin equation gives excellent agreement with DQMC. The data are for the Holstein limit ($\xi \to 0$).

bipartite square geometry. $S(\pi, \pi)$ signals the transition into a charge density wave (CDW) phase at low temperatures and half-filling. Because it is non-local, $S(\pi, \pi)$ poses a stringent test on equilibration and autocorrelation times.

We start with the Langevin and imaginary time discretization. The top panel of Fig. (1) shows the effect of the Langevin time step, $\mathrm{d}t$, on the value of the structure factor, $S(\pi, \pi)$, in the CDW ordered phase. We see that for $\mathrm{d}t \leq 0.015$, the error becomes linear in $\mathrm{d}t$. For $0.015 \leq \mathrm{d}t \lesssim 0.03$, the error is beyond the linear regime and increases rapidly and, eventually, for $\mathrm{d}t > 0.03$, the numerical integration is unstable. The stability limit, the largest allowed $\mathrm{d}t$, is set by the largest eigenvalue of the iterative process [21], while the critical slowing down is controlled by the ratio of the smallest to largest eigenvalues. The lower panel of Fig. 1 shows the effect of $\Delta\tau$, the imaginary time step, in comparison with DQMC, again in the CDW phase. We see that the two algorithms have comparable dependence on $\Delta\tau$, which is not surprising since this parameter appears in the same way in both. This also demonstrates that the Langevin algorithm gives the correct physical results. We note that these results were obtained with the Fourier accelerated algorithm (more below).

Having shown in Fig. 1 that the Langevin method gives results which are in agreement with DQMC, we now examine the approach to equilibrium. The left panel of Fig. 2 shows the evolution of $S(\pi, \pi)$ as a function of Langevin time for a system in the CDW phase. We see that, starting from a random phonon field, the unaccelerated evolution fails to find the CDW phase even long after the accelerated dynamics have converged. We also see that when the parameter choice is such that the system is in a CDW phase, convergence is helped by choosing an initial phonon field which has the CDW motif. If the parameters put the system in a disordered phase but the initial configuration is CDW, the checkerboard pattern will quickly melt away and the proper phase found. For these reasons, in what follows we will always use Fourier accelerated

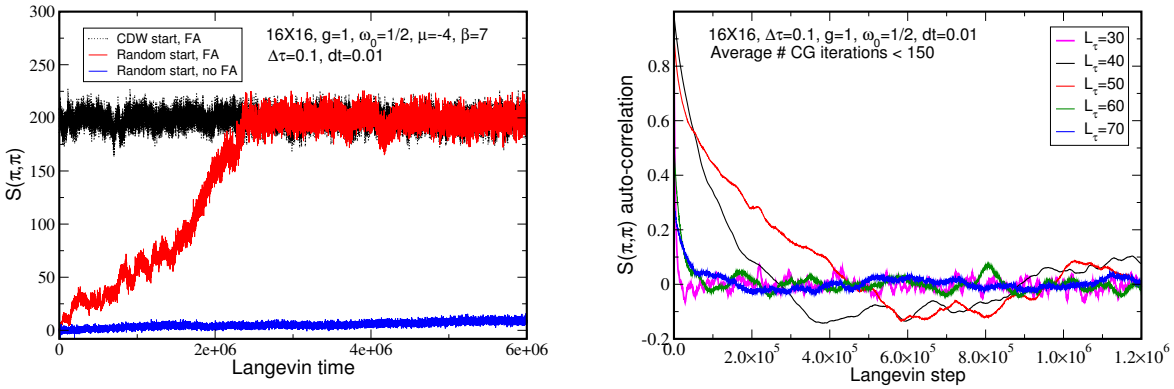

Figure 2. (Color online) Left: $S(\pi, \pi)$ as a function of Langevin time comparing Fourier acceleration (FA) with unaccelerated evolution. The red (FA) and blue (no FA) curves have the same random initial configuration of the phonon field. It is clear that for large systems FA is crucial for equilibration. The initial configuration for the black curve is CDW: The phonon field has an initial checkerboard configuration which triggers the CDW phase for the electrons. Right: The autocorrelation function of accelerated Langevin dynamics of the Holstein model for several β values. The relaxation time is longest for $L_\tau = 40$, 50 ($\beta = 4$, 5) near the critical temperature, $\beta \approx 4.5$.

dynamics.

The approach to equilibrium of the accelerated dynamics is illustrated by studying the autocorrelation time. We show this in the right panel of Fig. 2 for a 16×16 system at five values of β ranging from smaller than $\beta_c \approx 4.5$ to larger. We see that the longest relaxation times are $L_\tau = 40$, 50 ($\beta = 4$, 5) which are closest to β_c. The relaxation times for $\beta = 3$, 6, 7 are very short.

A very important question is how the numerical complexity scales with system size for fixed parameters. As mentioned above, DQMC scales as N_s^3 for contact interaction and as N_s^4 for long range interactions. Figure 3 shows the scaling of CPU time with system size for DQMC and Langevin for the case of contact interaction. For DQMC, the scaling is cubic, as expected, while for Langevin it is essentially linear for the two values of β shown. When the interaction is long ranged, we cut off the range of the interaction by keeping only interactions larger than 10^{-7} (a cutoff which can be adjusted to ensure physical observables are unaffected) which leads, again, to linear scaling for Langevin while DQMC scales as N_s^4. This means that as the system size increases, for fixed parameters, the number of bCG iterations necessary to calculate $M^{-1}\vec{g}$ remains essentially constant. This is very different from the behavior of bCG for other model. For example, for the Hubbard model, where the electron-electron interaction is decoupled via a Hubbard-Stratonovitch (HS) transformation, the number of iterations increases very rapidly with system size. We believe the difference in behavior for these two models is due to the fact that in the Hubbard model, the HS field does not have any intrinsic dynamics, it is not a physical field, and the properties of the matrix depend on the essentially random HS field. On the other hand, in the case of the Holstein model, the phonon field is physical and has its own dynamics, and in particular, has a second order derivative in the imaginary time direction (see Eq.(15)) which smooths out the phonon field. The eigenvalues of the matrix are, therefore, physical and depend on the parameters rather than the size of the system.

Two other interesting aspects of the number of bCG iterations needed are their dependence

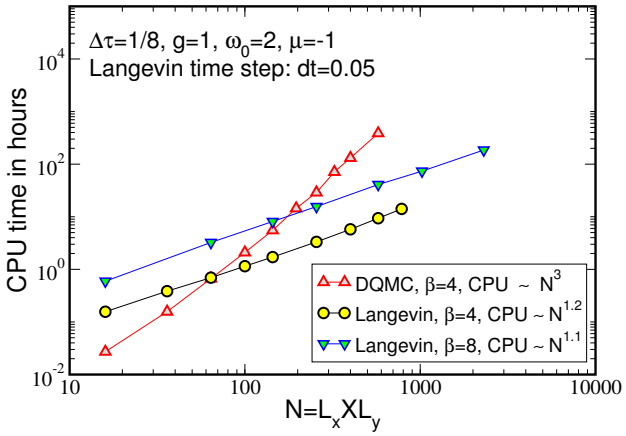

Figure 3. (Color online) CPU time versus system size in the Holstein limit ($\xi \to 0$) for DQMC and Langevin algorithms. DQMC scales as N_s^3 while Langevin scales essentially linearly for both values of β.

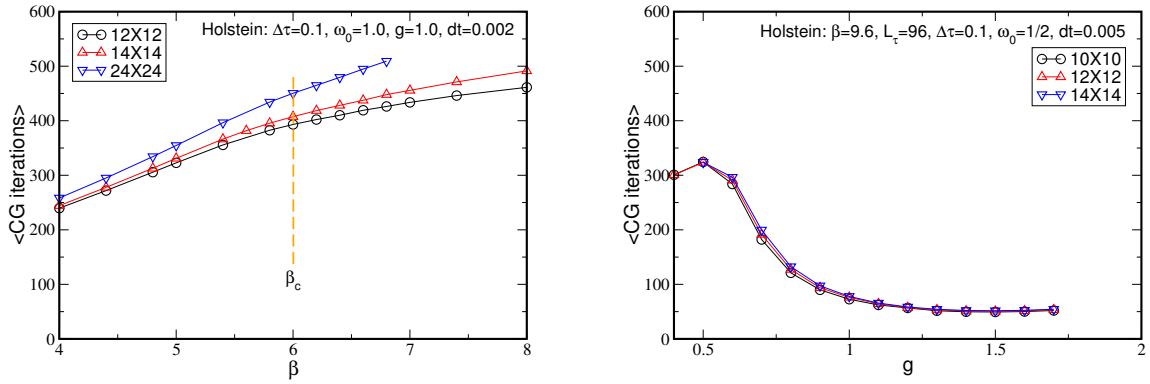

Figure 4. (Color online) Left: Dependence of the number of bCG iterations on the inverse temperature. Right: Dependence of the number of bCG iterations on the electron-phonon coupling constant, g: The number of iterations decreases with increasing g. Notice also the insensitivity to system size.

on β and on g. The left panel of Fig. 4 shows how this number scales with β while all other parameters are fixed. We see that as β_c is approached from the disordered side (small β) the number of iterations increases linearly and continues to do so for $\beta > \beta_c$ but with a smaller slope. The right panel of Fig. 4 shows the dependence of the number of iterations on the electron-phonon coupling constant, g. That the number of iterations decreases with increasing g leads to faster simulations and relaxation times since this behavior is connected with the eigenvalues of the fermion matrix. This behavior is in marked contrast with the Hubbard model, where increasing U leads to very rapid increase in the number of iterations. As discussed above, the difference in behavior is due to the fact that for the Hubbard model, the Hubbard-Stratonovitch field has no dynamics of its own whereas in the phonon model, the phonon momentum couples the field in the

imaginary time direction, leading to milder fluctuations. In addition to these considerations, one must choose a stopping criterion for the bCG iterations by choosing a tolerance for the solution. We have found that a tolerance of 10^{-4} to 10^{-5} ensures that errors are much smaller than stochastic and statistical errors and therefore do not affect the evaluation of physical quantities.

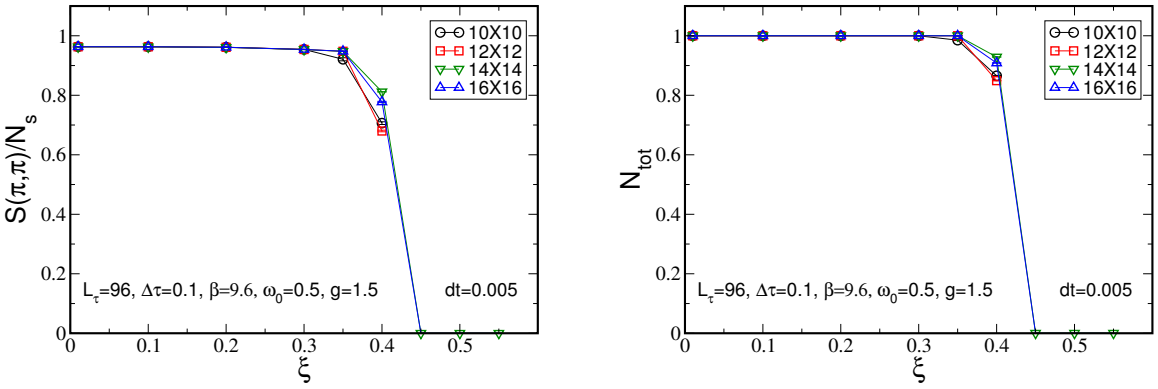

Figure 5. (Color online) Left: The structure factor, $S(\pi, \pi)$ as a function of the range of the interaction, ξ, keeping the chemical potential tuned to half filling. When the interaction is large enough, $S(\pi, \pi)$ drops to zero due to phase separation. Right: Same as left panel but showing the total number of particles. For $\xi \gtrsim 0.4$ the occupation vanishes, indicating phase separation. See also Fig. 6

.

4. Phase diagram: Long range interaction

Having validated the Langevin algorithm by demonstrating its convergence properties and agreeement with DQMC, we now use it to determine the ground state and finite temperature phase diagrams for the electron-phonon model with long range interaction. Such studies are basically unfeasible with DQMC due to the N_s^4 scaling of simulation time.

We fix $\omega_0 = 1/2$ and low enough temperature to obtain ground state values ($\beta = 9.6$), and study the properties of the system for different values of g and ξ to map the phase diagram. The left panel of Fig. 5 shows $S(\pi, \pi)$ as a function of the interaction range, ξ, for several system sizes. We see that for $\xi < 0.4$ the system is in a CDW phase which ends rapidly at $\xi \approx 0.4$. At the same the particle density suddenly drops from 1 (half filling) to 0, signaling phase separation. By making several such cuts in phase space, we map the ground state phase diagram, which is presented in Fig. 6.

In addition to ground state properties, the Langevin algorithm, like DQMC, provides information about finite temperature behavior. To determine the finite temperature phase transition from disordered at high temperature, to CDW as the temperature is lowered, we perform finite size scaling. Since the transition breaks a discrete (Z_2) symmetry, the phase transition is expected to be in the universality class of the two-dimensional Ising model. In the left panel of Fig. 7 we show the data collapse for $S(\pi, \pi)$ when Ising exponents are used. The collapse indicates that for the chosen parameters, the critical inverse temperature is $\beta_c = 6.01 \pm 0.05$. Repeating this kind of study for several values of ξ, we obtain $\beta_c(\xi)$ which is shown in the right panel. We see that as the range of the interaction increases, the tendency is to remain disordered down to lower temperatures before phase separation takes place at $\xi_c \approx 0.55$.

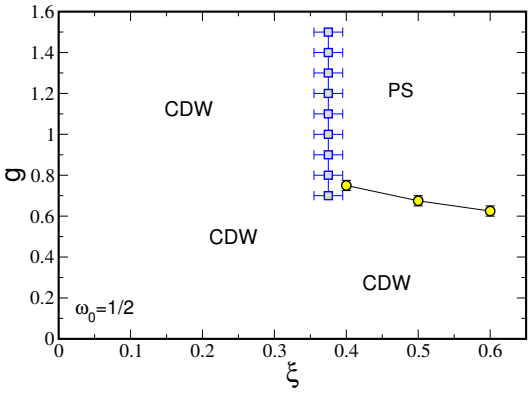

Figure 6. (Color online) The phase diagram in the g-ξ plane at half-filling and $\beta = 9.6$. The phonon frequency is fixed at $\omega_0 = 1/2$. At small ξ, the Holstein limit CDW correlations form. This occurs even at weak coupling owing to the Fermi surface nesting on the square lattice. As ξ increases, phase separation occurs.

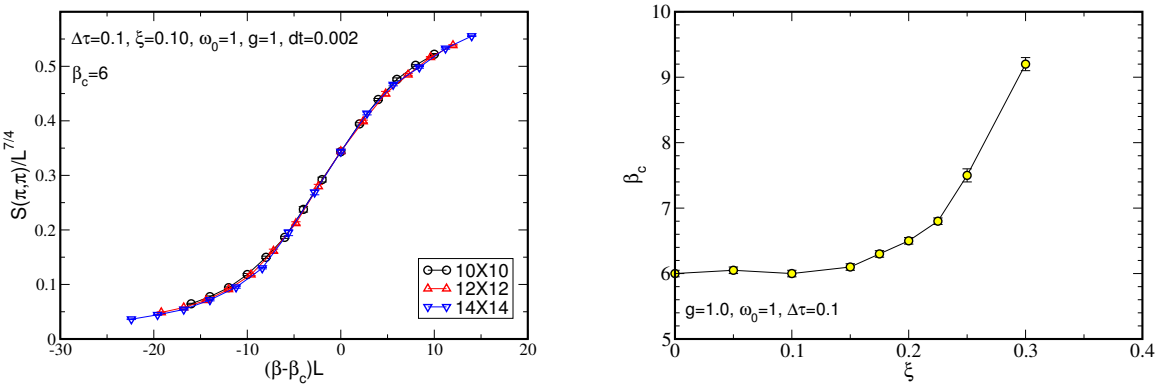

Figure 7. (Color online) Left: Scaling of the structure factor near the finite temperature transition from disordered to CDW phase. The error bars are smaller than the symbols. Right: The critical inverse temperature, β_c, as a function of the range of the electron-phonon interaction, ξ.

5. Summary

Langevin, and related, simulations of the Hubbard model have been attempted a number of times over the past several decades, with only limited success. In this paper we have shown that the smoothing effect of a phonon kinetic energy term makes these algorithms promising for electron-phonon problems. Specifically, we show that the iterative conjugate gradient solver converges in a reasonable number of steps, and that this number does not grow significantly with spatial size, inverse temperature, or coupling constant, as has bedeviled potential Hubbard model applications.

In addition to focusing on that fundamental bottleneck, we also explored various systematic effects, including those associated with discretization of the Langevin equation and of imaginary

time. These results, with associated comparisons with DQMC, both verify the correctness of the algorithm and identify the choices of dt and $\Delta\tau$ which provide acceptable systematic effects (e.g. smaller than the statistical sampling error bars).

There are two immediately promising applications of our method. The first is to the Holstein model in three dimensions, where T_c is not known because sufficiently large lattices are not accessible. The second is to problems with a long range (momentum dependent) electron-phonon coupling. Such couplings are of interest in explaining the behavior of a number of systems exhibiting novel CDW and superconducting phases [29, 30, 31, 32], but, like 3D, are out of reach of current approaches except in low dimension [33]. With the latter possibility in mind, we have presented results for the Frohlich model, and generated its phase diagram as a proof-of-principle calculation.

Another promising line of investigation concerns the Hubbard model and Holstein-Hubbard type of models. In the presence of the Hubbard U, the interaction term needs to be decoupled via the Hubbard-Stratonovitch (HS) transformation which introduces an additional auxiliary field which should be updated in the Monte Carlo simulation. In some cases, due to certain symmetries in the problem, the product of the two determinants resulting from tracing out the up and down fermionic operators, is positive definite and the simulation can proceed using well known methods such as DQMC. However, in most cases for $U > 0$, the product is not positive leading to the well known "fermionic sign problem". A possible way to deal with this problem is use a complex HS transformation and Langevin dynamics governed by the resulting complex effective action. This leads to the complex Langevin (CL) equation which has been investigated in the context of LGT[34]. In particular, this method was recently applied to the one-dimensional Hubbard model[35] and ultra-cold fermionic atoms with unequal masses[36]. For the Holstein-Hubbard model, where we now have two bosonic fields (the phonon and HS fields) the CL equation was shown to be efficient[37] in the interaction range $U > g^2/\omega_0$.

6. Acknowledgements

The work of RTS was supported by DOE-SC0014671. GGB is supported by the French government, through the UCAJEDI Investments in the Future project managed by the National Research Agency (ANR) with the reference number ANR-15-IDEX-01. We thank Steven Johnston, WeiTing Chiu, and Thomas Devereaux for useful conversations.

References

[1] Swendsen R H and Wang J-S, 1987 *Phys. Rev. Lett.* **58**, 86.
[2] Wolff U, 1989 *Phys. Rev. Lett.* **62**, 361.
[3] Hasenbusch M and Meyer S, 1990 *Phys. Lett.* **B241**, 238.
[4] Evertz H G, 2003 *Adv. in Phys.* **52**, 1.
[5] Sandvik A W, 1999 *Phys. Rev.* **B59**, R14157.
[6] Capogrosso-Sansone B, Söyler S G, Prokof'ev N, and Svistunov B, 2008 *Phys. Rev.* **A77**, 015602.
[7] Weber M, Assaad F F, and Hohenadler M, 2017 *Phys. Rev. Lett.* **119**, 097401.
[8] Scalettar R T, Scalapino D J, and Sugar R L, 1986 *Phys. Rev.* **B34**, 7911.
[9] Scalettar R T, Scalapino D J, Sugar R L, and Toussaint D, 1987 *Phys. Rev.* **B36**, 8632.
[10] Yamazaki I, Bai Z, Chen W, and Scalettar R T, 2009 *Numerical Mathematics: Theory, Methods and Applications* **2**, 469.
[11] Bai Z, Chen W, Scalettar R T and Yamazaki I, in "Multi-Scale Phenomena in Complex Fluids" edited by Thomas Y. Hou, Chun Liu and Jian-Guo Liu, pp. 1-110, Higher Education Press (2009).
[12] Broecker P, Carrasquilla J, Melko R G, and Trebst S, 2017 *Nature Sci. Rep.* **7**, 8823.
[13] Ch'ng K, Carrasquilla J, Melko R G, and Khatami E, 2017 *Phys. Rev.* **X7**, 031038.
[14] Costa N C, Hu W, Bai Z J, Scalettar R T, and Singh R R P, 2017 *Phys. Rev.* **B96**, 195138.
[15] Nomura Y, Darmawan A S, Yamaji Y, and Imada M, 2017 *Phys. Rev.* **B96**, 205152.
[16] Liu J, Qi Y, Meng Z Y, and Fu L, 2017 *Phys. Rev.* **B95**, 041101(R).
[17] Nagai Y, Shen H, Qi Y, Liu J, and Fu L, 2017 *Phys. Rev.* **B96**, 161102.
[18] Shen H, Liu J, and Fu L, arXiv:1801.01127.

[19] Liu J, Shen H, Qi Y, Meng Z Y, and Fu L, 2017 *Phys. Rev.* **B95**, 241104.
[20] Chen C, Xu X Y, Liu, J, Batrouni G G, Scalettar R T, and Meng Z Y, 2018 *Phys. Rev.* **B98**, 041102.
[21] Batrouni G G, Katz G R, Kronfeld A S, Lepage G P, Svetitsky B, and Wilson K G, 1985 *Phys. Rev.* **D32**, 2736.
[22] Batrouni G G, 1987 *Nucl. Phys.* **A461**, 351c.
[23] Davies C T H, Batrouni G G, Katz G R, Kronfeld A S, Lepage G P, Wilson K G, Rossi P and Svetitsky B, 1988 *Phys. Rev.* **D37**, 1581.
[24] Katz G R, Batrouni G G, Davies C T H, Kronfeld A S, Lepage G P, Rossi P, Svetitsky B, and Wilson K G, 1988 *Phys. Rev.* **D37**, 1589.
[25] Fröhlich H, 1954 *Adv. Phys.* **3**, 325.
[26] Scalettar R T, Scalapino D J, and Bickers N E, 1989 *Phys. Rev.* **B40**, 197.
[27] Blankenbecler R, Scalapino D J, and Sugar R L, 1981 *Phys. Rev.* **D24**, 2278.
[28] Risken H, Springer Series in Synergetics, Springer-Verlag (New York), 1996.
[29] Wang Y, Nakatsukasa Y, Rademaker L, Berlijn T, and Johnston S, 2016, *Supercond. Sci. Technol.* **29**, 054009.
[30] Weber F, Rosenkranz S, Castellan J-P, Osborn R, Hott R, Heid R, Bohnen K-P, Egami T, Said A H, and Reznik D, 2011, *Phys. Rev. Lett.* **107**, 107403.
[31] Swartz A G, Inoue H, Merz T A, Hikita Y, Raghu S, Devereaux T P, Johnston S, and Hwang H Y, 2018, PNAS 201713916.
[32] Devereaux T P, Shvaika A M, Wu K, Wohlfeld K, Jia C J, Wang Y, Moritz B, Chaix L, Lee W-S, Shen Z-X, Ghiringhelli G, and Braicovich L, 2016, *Phys. Rev.* **X6**, 041019.
[33] Hohenadler M, Assaad F F, and Fehske H, 2012, *Phys. Rev. Lett.* **109**, 116407.
[34] Aarts G, Seiler E, Sexty D, Stamatescu I-O, 2017, *J. High Energ. Phys.* **44**.
[35] Loheac C, Drut J E, 2017, *Phys. Rev.* **D95**, 094502.
[36] Rammelmüller L, Drut J E, Braun J, 2018, *J. Phys.: Conf. Ser.* **1041** 012006.
[37] Karakuzu s, Seki K, and Sorella S, arXiv:1808.07759.